PASJ: Publ. Astron. Soc. Japan , 1–??,
© 2014. Astronomical Society of Japan.

arXiv:1412.5528v2 [astro-ph.SR] 19 Dec 2014

Doppler Tomography by Total Variation Minimization

Makoto Uemura
Hiroshima Astrophysical Science Center, Hiroshima University, Kagamiyama 1-3-1, Higashi-Hiroshima, Hiroshima 739-8526
uemuram@hiroshima-u.ac.jp
Taichi Kato
Department of Astronomy, Kyoto University, Kitashirakawa-Oiwake-cho, Sakyo-ku, Kyoto 606-8502
Daisaku Nogami
Kwasan and Hida Observatories, Kyoto University, Yamashina-ku, Kyoto 607-8471
and
Ronald Mennickent
Universidad de Concepción, Departamento de Astronomía, Casilla 160-C, Concepción, Chile

(Received ; accepted)

Abstract

We have developed a new model of the Doppler tomography using total variation minimization (DTTVM). This method can reconstruct localized and non-axisymmetric profiles having sharp edges in the Doppler map. This characteristic is emphasized in the case that the number of the input data is small. We apply this model to real data of the dwarf novae, WZ Sge in superoutburst and TU Men in quiescence. We confirmed that DTTVM can reproduce the observed spectra with a high precision. Compared with the models based on the maximum entropy method, DTTVM provides the Doppler maps that little depend on the hyper-parameter and on the presence of the absorption core. We also introduce a cross-validation method to estimate reasonable values of a hyperparameter in the model by the data itself.

Key words: accretion, accretion disks — methods: data analysis — novae, cataclysmic variables

1. Introduction

Doppler tomography (DT) is a widely-used method in the field of binary systems (Marsh, Horne 1988). It reconstructs an emission-line intensity map in the velocity space (Doppler map) from the temporal variation of the line profile. This method is valid in the case that the line forming region co-rotates with the orbital motion. Such a condition is indeed a good approximation for real data of the emission line of the accretion disk in cataclysmic variables (CVs) (Smak 1981). A number of studies using DT have revealed characteristic features of accretion disks in CVs: spiral patterns, stream-impact region, and also the emission from the secondary star (e.g. Marsh et al. 1990; Steeghs et al. 1997; Schwope et al. 1997).

DT is an ill-posed inverse problem in most cases. A filtered back-projection method provides a way to solve the problem. It masks high frequency components in the Doppler maps in order to uniquely determine the solution. The other way is to introduce regularization terms in addition to the likelihood term. The maximum entropy method (MEM) has been used for DT. The DT with MEM determines the solution by maximizing the information entropy over the default image. One can choose an appropriate default image, for example, axi-symmetric or Gaussian blur image. The comparison between the back-projection method and MEM is reported in Marsh (2001).

In general, those DT methods tend to smear out localized and sharp-edge profiles in the Doppler map because such profiles have high frequency components which make the entropy low. On the other hand, they are expected in accretion physics, such as spiral shocks and hot spots. It has been reported that there are significant residuals between the observed and model spectra that are obtained from DT (e.g. Tappert et al. 2003). It is, however, unclear whether the large residuals are caused by the emission components which violate the basic assumption that the emission is isotropic and optically thin. Alternatively, it may be caused by regularization terms which are ill-suited for the real disk.

In this paper, we propose a new DT by total variation minimization (TVM). TVM has received attention in the field of image reconstruction because it can reconstruct sharp-edge features by making the image sparse in its gradient domain. In section 2, our model of DT by TVM (DTTVM) is described. In section 3, several experiments of DTTVM are shown for both artificial and real data. In section 4, we shortly discuss the treatment of absorption components in our model, and summarize our findings in section 5.

2. Model

DT is a method to reconstruct the Doppler map, i.e., the intensity map in the velocity space (v_x, v_y). The coordinate system in our model is the same as previous models of DT (Marsh, Horne 1988): The radial velocity $v_{\rm R}$ of a point (v_x, v_y) in the map is represented as:

$$v_{\rm R} = -v_x \cos\phi + v_y \sin\phi, \tag{1}$$

where ϕ is the orbital phase that can be calculated from the observation time and the ephemeris of the binary system. Suppose that there are M data given by $\boldsymbol{d} = \{d_0, d_1, \cdots, d_M\}$. The i-th element of $\boldsymbol{d}$, d_i, is the flux at a radial velocity $v_{\mathrm{R},i}$ and phase ϕ_i. Also suppose $n \times n = N$ points in the Doppler map given by $\boldsymbol{s} = \{s_{0,0}, s_{0,1}, \cdots, s_{n,n}\}$. The j-th element in the map has the coordinate of $(v_{x,j}, v_{y,j})$ and intensity of s_j. The radial velocity at ϕ_i and $(v_{x,j}, v_{y,j})$ can be calculated from equation (1) and represented as $v_{\mathrm{R},ij}$.

The goal of DT is to estimate $\hat{\boldsymbol{s}}$ from observations according to

$$\hat{\boldsymbol{s}} = \arg\min_{\boldsymbol{s}} \left\{ \frac{1}{M} \|\boldsymbol{d} - A\boldsymbol{s}\|_2^2 + \frac{\lambda}{N} \Phi(\boldsymbol{x}) \right\}. \quad (2)$$

The first term in the right side is the least-square term, and the second term is the regularization term which consists of a hyperparameter λ and a function Φ. In equation (2), A is a $M \times N$ matrix whose element depends on the phase, radial velocity, and instrumental response. For the response function, we assumed a Gaussian profile with a variance σ^2. An element of A, a_{ij}, is then given by

$$a_{ij} = \frac{1}{\sqrt{2\pi\sigma^2}} \exp\left\{ -\frac{(v_{\mathrm{R},i} - v_{\mathrm{R},ij})^2}{2\sigma^2} \right\}. \quad (3)$$

Here, σ means a width of the instrument line broadening. The sampling interval of spectra is usually designed to be smaller than the broadening width in astronomical spectrographs. Hence, σ corresponds to a spectral resolution in most cases of actual observations.

TVM provides a method to solve ill-posed problems. The isotropic total variation of the map, $\Phi_{\mathrm{TVM,iso}}$, is defined as

$$\Phi_{\mathrm{TVM,iso}}(\boldsymbol{s}) = \sum_{i,j} \sqrt{(s_{i+1,j} - s_{i,j})^2 + (s_{i,j+1} - s_{i,j})^2}. \quad (4)$$

The anisotropic total variation is

$$\Phi_{\mathrm{TVM,aniso}}(\boldsymbol{s}) = \sum_{i,j} |s_{i+1,j} - s_{i,j}| + |s_{i,j+1} - s_{i,j}|. \quad (5)$$

$\Phi_{\mathrm{TVM,iso}}$ is used as Φ in equation (2) in this paper. We confirmed that the model with $\Phi_{\mathrm{TVM,aniso}}$ generates almost the same results as that with $\Phi_{\mathrm{TVM,iso}}$.

We use the TwIST algorithm to estimate $\hat{\boldsymbol{s}}$ in equation (2) (Bioucas-Dias, Figueiredo 2007b; Bioucas-Dias, Figueiredo 2007a).[1] This is a kind of Iterative Shrinkage/Thresholding (IST) algorithm, or sometimes called as the proximal gradient method. IST is an algorithm for minimization problems of a function that is a sum of a differentiable convex function and non-differentiable, but simple-form convex function. The least-square and TVM terms correspond to those two functions in the present case. IST solves the problem by a combination of the proximal point method and gradient method: One step consists of a gradient step for the least-square term and a proximal point correction step for the TVM term. The TwIST algorithm is a two-step iterative version of IST, enabling a faster convergence than IST. In the present case, the iteration algorithm of TwIST is,

$$\begin{aligned} \boldsymbol{s}_{t+1} = {} & (1-\alpha)\boldsymbol{s}_{t-1} + (\alpha - \beta)\boldsymbol{s}_t \\ & + \beta \Psi_\lambda \left(\boldsymbol{s_t} + A^T(\boldsymbol{d} - A\boldsymbol{s_t}) \right), \end{aligned} \quad (6)$$

where Ψ_λ is the proximal operator. For TVM, there is no closed form of Ψ_λ, and the iterative method proposed in Chambolle (2004) is used. In the present case, we used $\alpha = 1.44$ and $\beta = 0.92$.The intensity $s_{i,j}$ in the Doppler map can be negative in the present model.

The calculation code of DTTVM is available at our web site.[2] As can be seen in equation (2), the present model assumes that the noise follows a symmetric probability distribution, like a Gaussian distribution, and that all observations are yielded with the same variance. The least-square term in equation (2) should be replaced by the least-square term weighted with each observation error if the data quality varies widely.

3. Results

3.1. Experiments using artificial data

We make artificial Doppler maps, then simulate line-profile variations, and reconstruct the maps from the simulated data. First, we test DTTVM on a case in which the number of the data is larger than the number of pixels of the Doppler map. Here, the number of the data means the dimension of $\boldsymbol{d}$ in equation (2), that is, the number of all data points of the flux in all v_{R} and ϕ. The artificial map contains three spot structures, as shown in the upper left-most panel of figure 1. Spectra were calculated from this map with a phase interval of 0.01 and a radial velocity interval of $10\,\mathrm{km\,s^{-1}}$ between -2000 and $+2000\,\mathrm{km\,s^{-1}}$. No noise was added to the simulated spectra. We assumed σ in equation (3) to be $100\,\mathrm{km\,s^{-1}}$, which corresponded to $235\,\mathrm{km\,s^{-1}}$ in full-width of half maximum (FWHM) of the Gaussian profile. As a result, the number of the input data is 40100. Using this data, DTTVM estimates $64 \times 64 = 4096$ elements of the Doppler map. Figure 1 shows the results. Three different values of the hyperparameter, λ were used to see the dependence on it. Panels (a) and (c) show the cases of the smallest and largest λ.

As can be seen in figure 1, the residuals of the model from the assumed spectra are smaller for smaller λ. This behavior can be easily understood because the solution becomes close to that determined by the least-square term in the case of very small λ in equation (2). No major difference can be seen in all three estimated Doppler maps.

We also performed MEM reconstructions using the same map as figure 1. We used two calculation codes: `doppler` developed by T. Marsh[3] and `dopp` developed by H. Spruit (Spruit 1998)[4]. For the MEM models, the regularization term,

[1] ⟨http://www.lx.it.pt/~bioucas/TwIST/TwIST.htm⟩

[2] ⟨http://home.hiroshima-u.ac.jp/uemuram/dttvm/⟩

[3] ⟨http://deneb.astro.warwick.ac.uk/phsaap/software/doppler/html/OVERVIEW.h

[4] ⟨http://www.mpa-garching.mpg.de/~henk/⟩

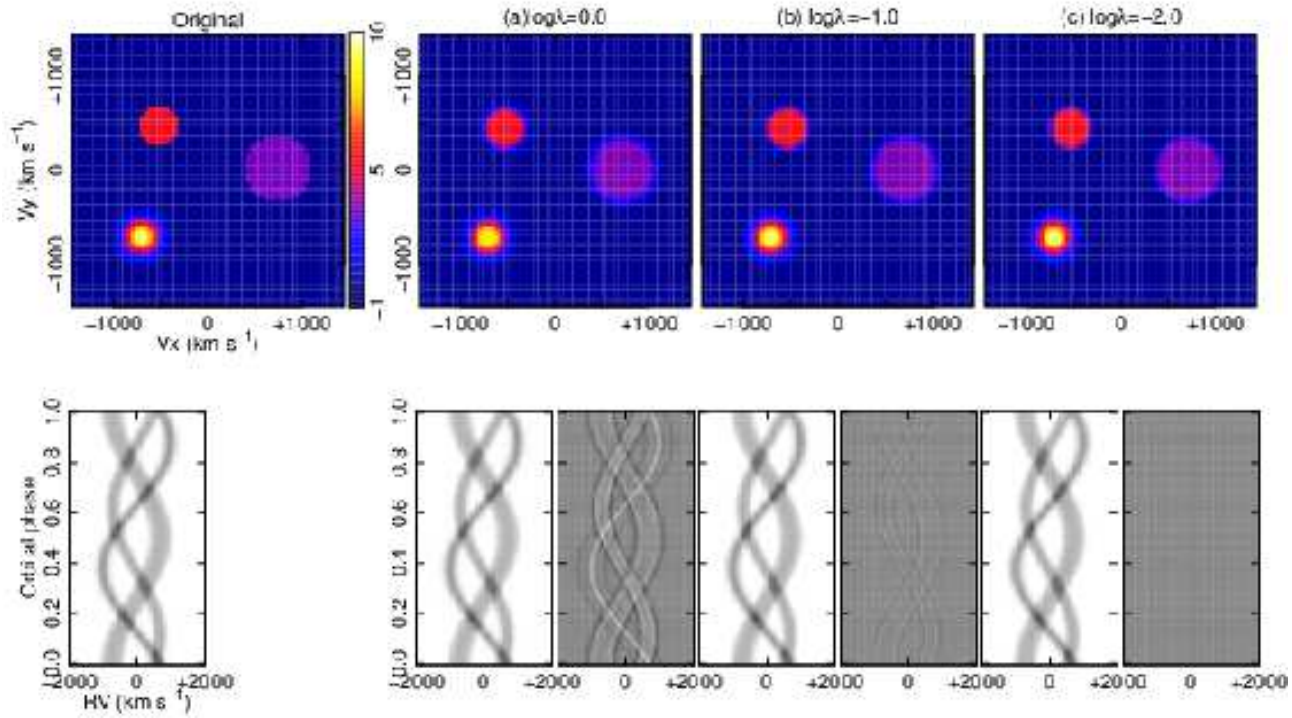

Fig. 1. Results of DTTVM using an artificial map having three spots. The artificial map is depicted in the upper left-most panel. The simulated spectrum from the map is shown in the lower left-most panel. The spectra were calculated with a phase interval of 0.01 and a radial velocity interval of 10 $\mathrm{km\,s^{-1}}$ between -2000 and $+2000$ $\mathrm{km\,s^{-1}}$. Three sets of results are shown with different values of λ, which are indicated by the top of each panel. For each set, the estimated Doppler map is shown in the upper panel. The lower left and right panels are the model spectra and residuals between the original and model spectra, respectively. The Doppler maps consist of 64×64 bins. The intensities of the assumed spots are 10, 5, and 3 at the peak of the lower left Gaussian profile and in the upper left and right flat-top regions, respectively. The intensity is 0 outside these spots.

$$\Phi_{\mathrm{MEM}}(\boldsymbol{s}) = -\sum_{i,j}\left(s_{i,j}\ln\frac{s_{i,j}}{\chi_{i,j}} + \chi_{i,j}\right) \tag{7}$$

is used, where $\chi_{i,j}$ is the default image. According to Spruit (1998), the standard default image is that created from $\boldsymbol{s}$ by a Gaussian smearing, which is used in `dopp`. We set the same default image also in `doppler`. We confirmed that those two MEM codes provided almost consistent results (except for the data of WZ Sge, see subsection 3.2). All MEM results presented in this paper are those obtained by `doppler`. Since we focus on the reconstruction of sharp-edged profiles, we used a small smearing factor in `doppler` (the parameter, BLURR= 1.0). We calculated the input spectra from the assumed maps by the method defined in `doppler`.

Figure 2 shows the MEM results. In the code `doppler`, the parameter χ^2_{aim}, or CAIM in the code, corresponds to the hyper-parameter in the MEM model. As in figure 3, we show three sets of results obtained by different χ^2_{aim}, which are shown in the top of each panel. All three results are consistent with those in the TVM case. We calculated the RMS of the residuals between the model and data of spectra. In cases (c) of both figures 1 and 2, RMS are below 0.005, corresponding to 3 % of the peak flux in the spectra. Those two experiments demonstrate that both TVM and MEM codes can reproduce the Doppler map when the number of the data is large.

Next, we test DTTVM in the case that the number of data is smaller than the pixels of the Doppler map. Spectra were calculated from the same map in figure 1 with a phase interval of 0.05 and a radial velocity interval of 100 $\mathrm{km\,s^{-1}}$. The instrument response is the same as the last case: $\sigma = 100$ $\mathrm{km\,s^{-1}}$, or FWHM = 235 $\mathrm{km\,s^{-1}}$. The number of the input data is 820, which is less than the number of elements of the estimated map, that is, $64 \times 64 = 4096$. The results are shown in figure 3. DTTVM successfully reproduced the original map in all three cases. In the assumed Doppler map, the upper two spots have sharp-edge and flat-top profiles with different size and intensity. The lower left spot has a Gaussian profile. This difference in the structure is properly reproduced in the estimated maps in figure 3.

Figure 4 is the result of MEM using the same configuration of the data as in figure 3. The map of case (a) underestimates the flux of all spots. As a result, we can see significant residuals between the model and assumed spectra. Smaller χ^2_{aim} leads to smaller spectral residuals, while more spurious structures appears in the Doppler maps, as shown in cases (b) and (c). The map is filled by noise in case (c) and also cases with further smaller χ^2_{aim}.

The results shown in figures 1–4 suggest that DTTVM can reconstruct both sharp-edge and smooth profiles in

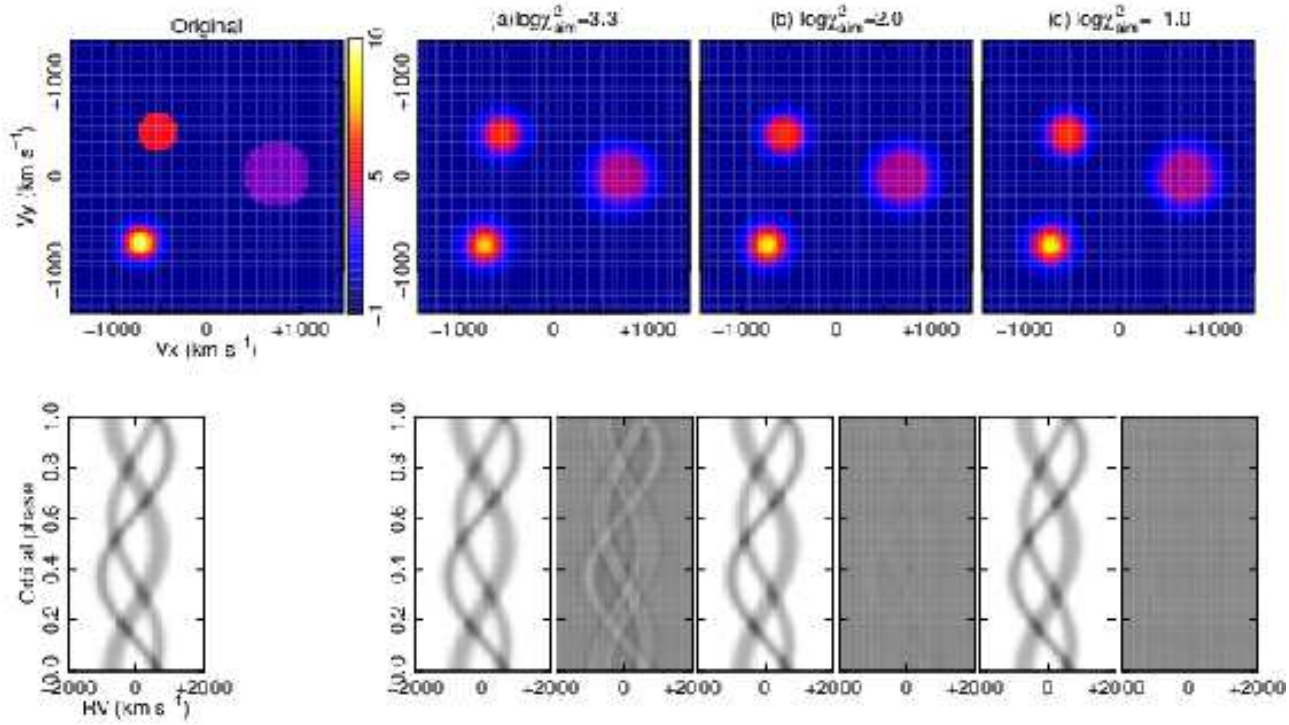

Fig. 2. As in figure 1, but for the MEM case. The ranges of the gray scale of the model and residual spectra are common in that in figure 1.

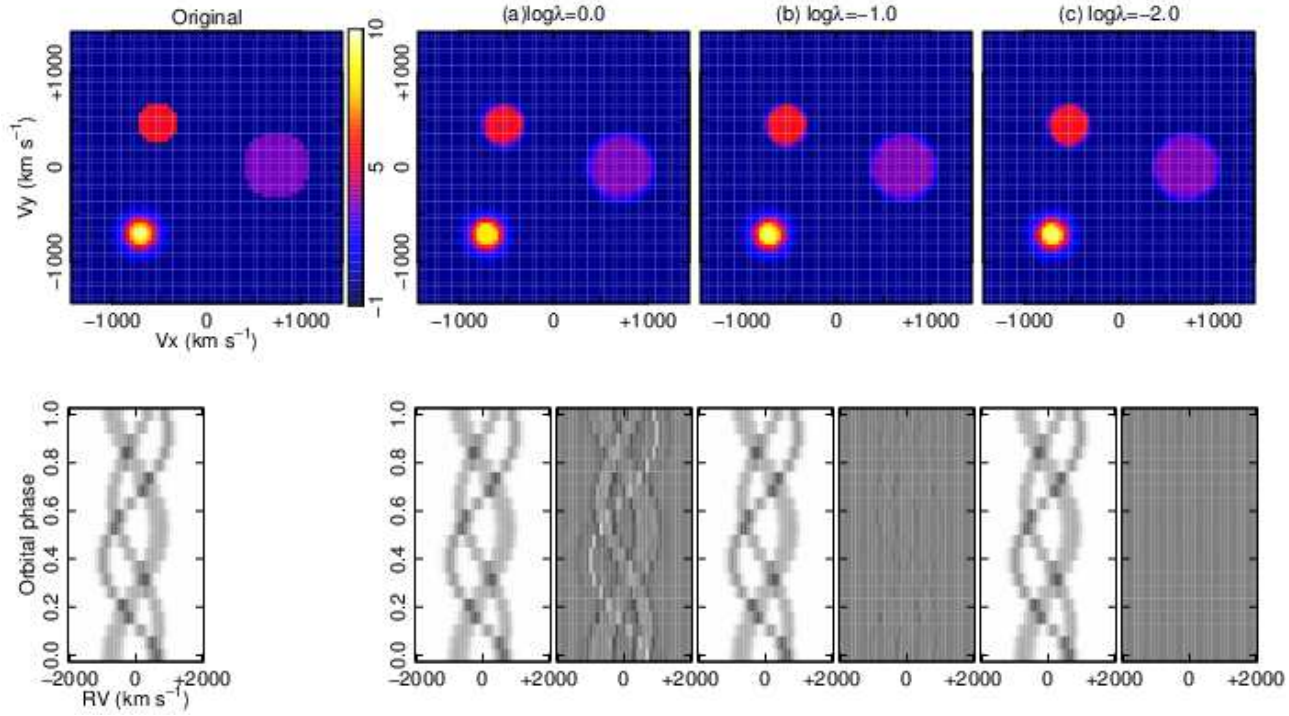

Fig. 3. As in figure 1, but for the small number of input data. The spectrum was calculated with a phase interval of 0.05 and a radial velocity interval of 100 km s^{-1} between −2000 and +2000 km s^{-1}.

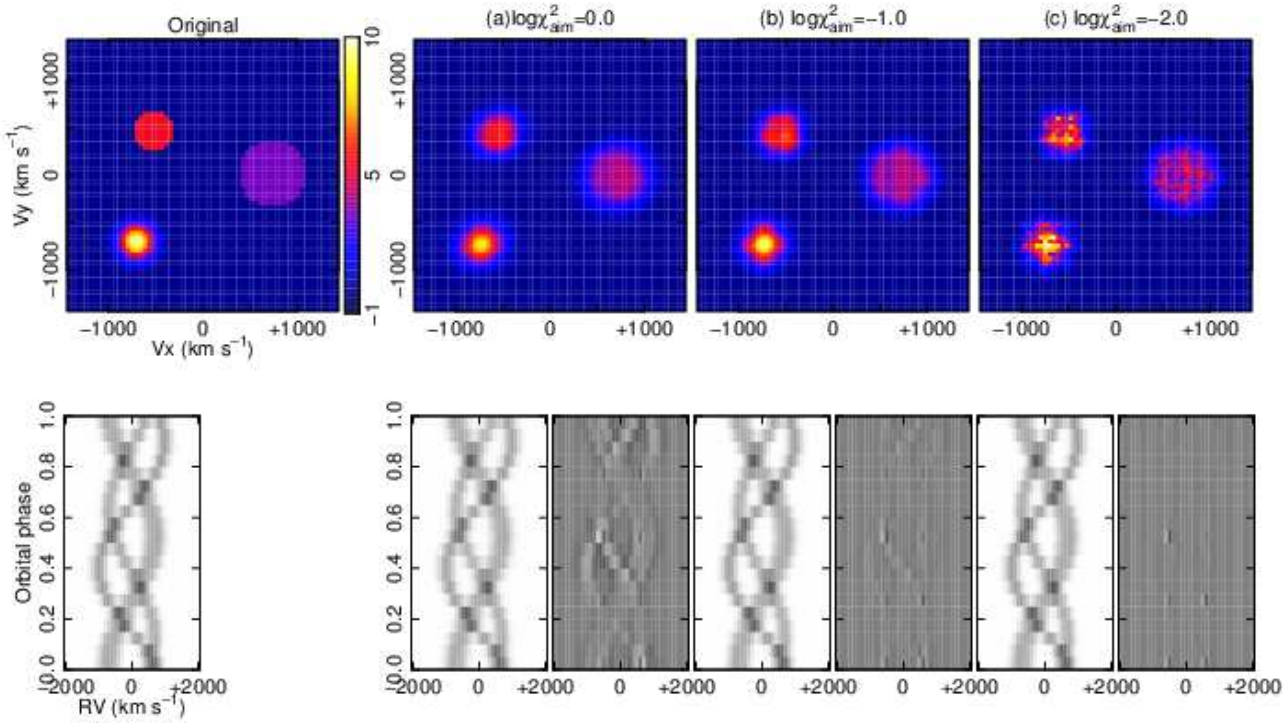

Fig. 4. As in figure 3, but for the MEM case. The color scales of the Doppler maps are different in each case, but the model spectra and residuals are shown in the same scale for each. The ranges of the gray scale of the model and residual spectra are common in that in figure 3.

the Doppler map. This characteristic is emphasized compared with the MEM method in the case that the number of data is small.

We see another examples of the DTTVM reconstruction using artificial maps in the case of the same small data set used in figure 3, in which a phase interval is set to be 0.05 and a radial velocity interval is set to be $100\,\mathrm{km\,s^{-1}}$. Figure 5 shows the case of the Doppler map having disk and spot features. In the accretion disks of CVs, the line intensity is proposed to be a function of radius, $I \propto r^{-3/2}$ (Young et al. 1981). In conjunction with the Kepler rotation, $v \propto r^{-1/2}$, we set a small gradient for the disk intensity, $I \propto r^{1/3}$ in those maps. The spot has a constant intensity. The reconstructed maps show similar behavior as in the previous case; the spot intensity is underestimated in a low λ case, and the residuals of spectra are smaller in higher λ cases. The small intensity gradient is also reconstructed in case (b) and (c).

Figure 6 shows the case of the Doppler map having two-armed spiral patterns. The upper spiral has a constant intensity, and the lower has an intensity gradient with an exponential form. The reconstructed maps by TVM again shows similar behavior that the last cases. In this case, however, they fail to reconstruct fine structures, such as a tail of the spirals and the intensity gradient in the lower spiral, while sings of their features are still seen in the maps. The low quality of those fine structures is due to the finite spectral resolution of the simulated spectra. The resolution was set to be $100\,\mathrm{km\,s^{-1}}$. The structure smaller than this resolution lost its information in the simulated spectra, as a result, it cannot be recovered.

3.2. Application for real data

We apply DTTVM to the data of the dwarf nova, WZ Sge taken on the 10th day of the superoutburst in 2001 (Nogami, Iijima 2004). The number of the data point is 630. We estimated a 64×64 Doppler map using the data. The data having radial velocities between -200 and $+200\,\mathrm{km\,s^{-1}}$ were excluded because of the prominent absorption core which violates the model assumption of the Doppler tomography. The velocity resolution was $270\,\mathrm{km\,s^{-1}}$, which was used as σ in equation (3). Figure 7 presents the Doppler maps and model spectra. The results were computed using $\log_{10}\lambda$ of (a) -2.2, (b) -3.2, and (c) -5.2. All Doppler maps exhibit a disk feature having non-axisymmetric intensity distribution. Its entire structure is circular in case (a), but elliptical in cases (b) and (c). The model spectra reproduce the observed one with a high precision in cases (b) and (c), while we can see several significant components of residuals in case (a).

Figure 8 is the result of the Doppler tomography for the same data calculated using MEM. In case (a), the bright region appears around the upper-right area in the Doppler map, while the map is so simple that the spectral residuals of the model from the data is large. Reducing χ^2_{aim} leads to reducing the residuals, as can be seen in case (b). In addition to the upper-right region, the map has another bright region at $(v_x, v_y) \sim (0, 500)$ and a weak sign of a

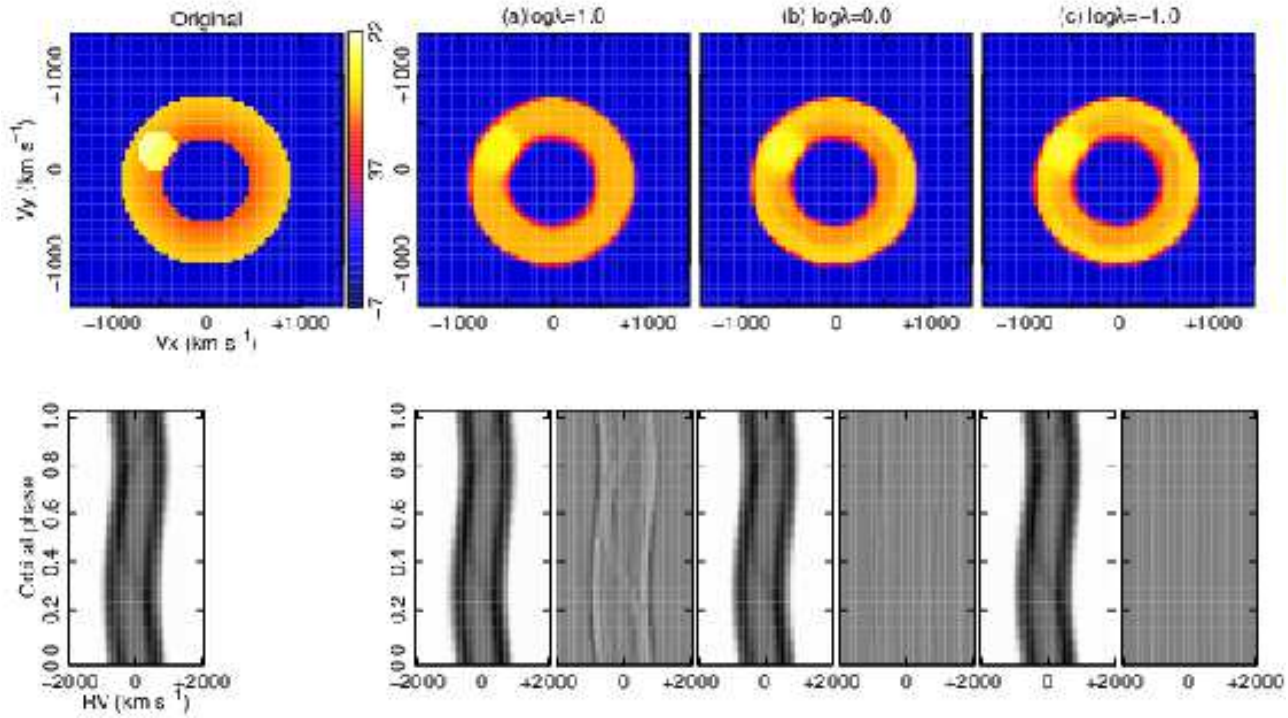

Fig. 5. As in figure 3, but for the artificial map having a disk and spot.

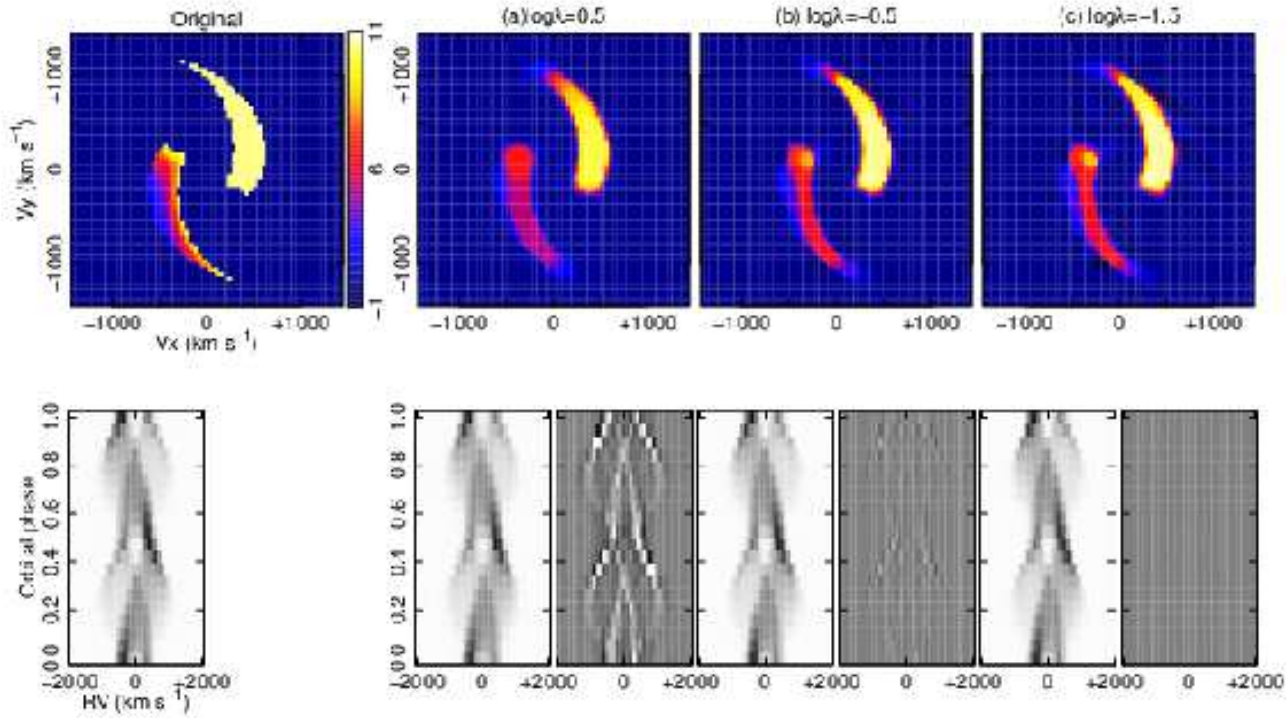

Fig. 6. As in figure 3, but for the artificial map having spiral patterns.

circular disk. Steeghs (2004) performed Doppler tomography with MEM also using data of WZ Sge in outburst. Their Hβ map on the ninth day of the superoutburst has similar features to case (b). In our MEM analysis, noisy structures appear in case (c) and calculations with further smaller $\chi^2_{\rm aim}$, but they are evidently artifacts. In cases (a) and (b), there are significant residuals of the spectral data at $+500\,{\rm km\,s^{-1}}$ for phase 0.75. This feature has counterparts at $-500\,{\rm km\,s^{-1}}$ for phase 0.25. Another local residuals can be seen at $-500\,{\rm km\,s^{-1}}$ for phase 0.8.

Table 1 lists the RMS of residuals between the model and observed spectra of WZ Sge for both cases of TVM and MEM. Note that the spectra are normalized by the continuum level, and the average and maximum fluxes are 0.06 and 0.26, respectively. As shown in this table, the RMS obtained by DTTVM are smaller than those by MEM. A reason for the high quality reproduction of DTTVM may be the constraint condition of $\boldsymbol{s}$ in equation (2): the elements of $\boldsymbol{s}$ can be negative in our model, but must be positive in the available MEM codes. The line profile observed in CVs frequently has an absorption core. This absorption is formed by the outermost, low radial-velocity region of the disk where the line emission is partially optically-thick. Our model can fit the absorption core by taking negative values of $\boldsymbol{s}$, which is prohibited in the MEM codes. The low velocity regions between -200 and $+200\,{\rm km\,s^{-1}}$ are masked for the current analysis, while it may not be enough to mask the entire absorption component.

Then, we added a Gaussian component to the data so that the negative pixels at the low velocity area in the Doppler map disappears (Marsh et al. 1990; Harlaftis, Marsh 1996). The Gaussian component has a standard deviation of $300\,{\rm km\,s^{-1}}$ and the peak (normalized) flux of 0.25, centering at a radial velocity of $0.0\,{\rm km\,s^{-1}}$. These are minimum values by which the central negative pixels disappear in the Doppler map estimated by DTTVM. We analyzed the modified data using DTTVM and the MEM code. The results are shown in figures 9 and 10, respectively.

The DTTVM results (figure 9) are consistent with those in figure 7: The brightest spot lies at $(v_x, v_y) \sim (0, +500)$, and the lower-right area in the disk region is also bright in the Doppler maps. There are several high-velocity areas having very low intensity, or negative values in some pixels in figure 9. They are probably due to over-fitting of the noise in the data. They are so localized that they may make narrow absorption-like effect on the spectra, but do not change the entire structure of the Doppler map.

In the case of the MEM (figure 10), especially in case (b), the Doppler maps have a different feature from those in figure 8. In addition to the brightest spot at $(v_x, v_y) \sim (0, +500)$, we can see a weak sign of the bright region in the lower-right area of the map. This feature is rather similar to the DTTVM results. In addition, the RMS of the model spectra to the data is small comparable to the DTTVM values, as shown in table 1. We note that these behavior was only seen in the code `doppler`, and not in `dopp`. In the case of `dopp`, the Doppler maps little depend on the presence or absence of the absorption component, and the upper-right disk area is always the brightest, as in figure 8.

We also analyzed the data of a dwarf nova TU Men in quiescence. The data was reported in Mennickent (1995). The total number of the data point is 5293. We estimated the 80×80 Doppler map. Figure 11 shows the result obtained by DTTVM. The results were computed using λ of (a) 5.0, (b) 0.5, and (c) 0.1. In cases (b) and (c), a sign of the secondary star can be seen at $(v_x, v_y) \sim (0, 100)$ in the Doppler map, as well as a disk structure. Tappert et al. (2003) also report the result of the Doppler tomography with MEM using the same data. Their result is consistent with figure 11, except for spectral residuals. Their result shows several rotating components in the residuals. They propose that the residuals are due to the anisotropy of the emitting region. However, our result exhibits no major residual, indicating that the MEM method failed to recover localized components.

3.3. Cross-validation method to determine a hyperparameter, λ

DTTVM has a hyperparameter, λ, as shown in equation (2). The reasonable λ can be estimated by the data itself using the cross-validation method. In the K-fold cross-validation, the data is divided into K roughly equal parts, $\boldsymbol{y}_k$ ($k = 1$–K). For each k, the training data is defined as the all $K-1$ data except for the validation data, $\boldsymbol{y}_k$. The optimization of the model using the training data gives $\hat{\boldsymbol{x}}_{k,\lambda}$ at a certain λ. The prediction reliability of the model is evaluated with mean square errors (MSE);

$$E(\lambda) = \frac{1}{K}\sum_{k=1}^{K} E_k(\lambda) \tag{8}$$

$$E_k(\lambda) = \frac{1}{N_k}\|\boldsymbol{y}_k - A\hat{\boldsymbol{x}}_{k,\lambda}\|_2^2, \tag{9}$$

where N_k is the number of the validation data, $\boldsymbol{y}_k$. The MSE, $E(\lambda)$ can be the minimum value at a certain λ. In a large λ regime, the least-square term can be large, which leads to a large $E(\lambda)$. In a small λ regime, on the other hand, the model can reproduce even noises in the training data, and thereby have a low prediction reliability, and lead to a large $E(\lambda)$. This situation is known as model over-fitting. Thus, we can determine a reasonable range of λ by the behavior of $E(\lambda)$. We set $K = 10$ in this paper.

Figure 12 shows $E(\lambda)$ against λ, calculated using the data of TU Men. $E(\lambda)$ clearly takes the minimum at $\lambda \sim 0.1$. The vertical bars associated with $E(\lambda)$ represent the standard error of $E_k(\lambda)$ ($k = 1$–10). Hence, there is an uncertainty of λ at which $E(\lambda)$ takes minimum, in other words, for the best model. Instead of the model with the minimal $E(\lambda)$, we can take the simplest model whose $E(\lambda)$ is within one standard error of the minimal $E(\lambda)$. This is sometimes called as the "one standard error rule". The three Doppler maps shown in figure 11 corresponds to the results for $\lambda = 5.0$, 0.5, and 0.1. The model with $\lambda = 5.0$ is so simple, or sparse in the gradient domain that $E(\lambda)$ is large. The models with $\lambda = 0.5$ and 0.1 correspond to those

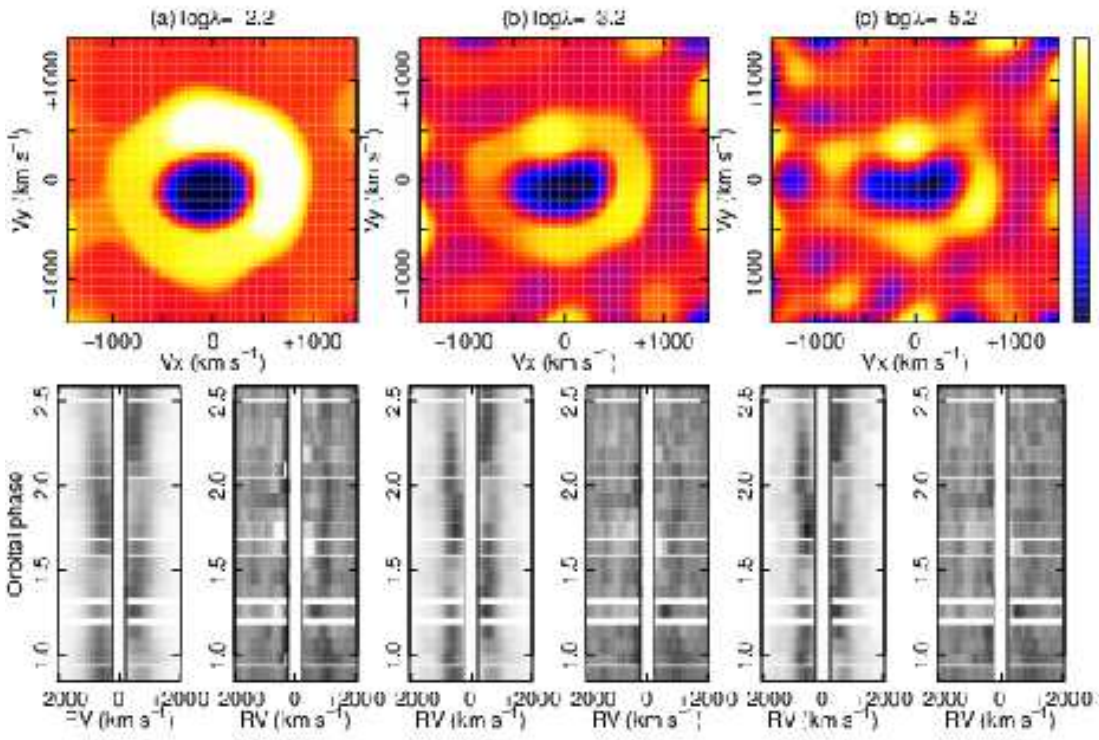

Fig. 7. Results of DTTVM for the data of WZ Sge. Upper panels: the Doppler maps. Lower left and right panels: the model spectra and residuals between the model and observed spectra, respectively. The three sets of the panels were calculated with different λ, which are indicated in the figure. The Doppler maps consist of 64×64 bins. The ranges of the gray scale of the model and residual spectra are common in that in figure 8. The data in the masked area in the spectra between -200 and $+200\,\mathrm{km\,s^{-1}}$ was not used for the Doppler tomography because the contamination of the absorption core is strong.

Table 1. RMS of the residuals between the model and observed spectra of WZ Sge.

Model	Figure number	RMS		
		case (a)	case (b)	case (c)
TVM	7	0.023	0.019	0.017
MEM	8	0.031	0.024	0.020
TVM (absorption core corrected)	9	0.022	0.019	0.017
MEM (absorption core corrected)	10	0.022	0.018	0.016

obtained by the one standard error rule and minimal $E(\lambda)$, respectively. We can consider that the case for $\lambda = 0.5$ is the most reasonable model for the data.

Figure 13 shows the same as figure 12, but for the data of WZ Sge. In this case, MSE takes the minimum at $\log_{10}\lambda = -5.2$, while the increasing trend of $E(\lambda)$ in small λ is not prominent compared with the case of TU Men. In figure 7, we show the results for $\log_{10}\lambda = -2.2$, -3.2, and -5.2, that is, under-fitted model, model with λ for the one standard error rule, and model with the minimal $E(\lambda)$. As in the case of TU Men, we can consider that panel (b) of figure 4 is the most reasonable model.

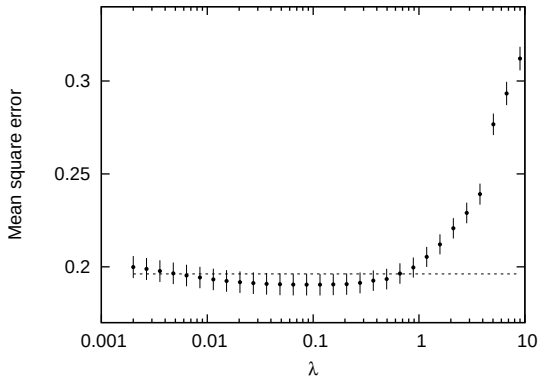

Fig. 12. The mean square errors between the model and validation data against a hyperparameter, λ for the data of TU Men.

4. Discussion

As demonstrated in subsection 3.1, DTTVM can reconstruct both sharp-edge and smooth profiles in the Doppler

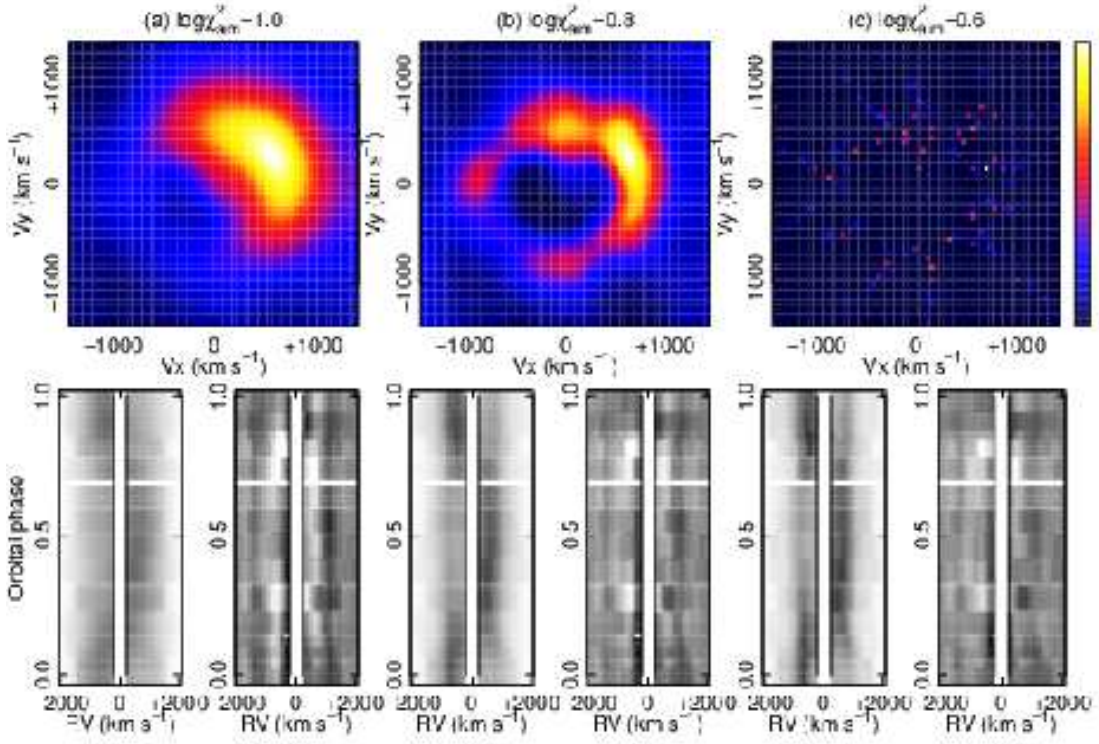

Fig. 8. As in figure 7, but for the MEM case. The color scales of the Doppler maps are different in each case. The ranges of the gray scale of the model and residual spectra are common in that in figure 7. The orbital phase in the trailed spectra is set from 0.0 to 1.0, not as in figure 7. This is a feature of the calculation code, and the spectra were not binned in the phase for the analysis.

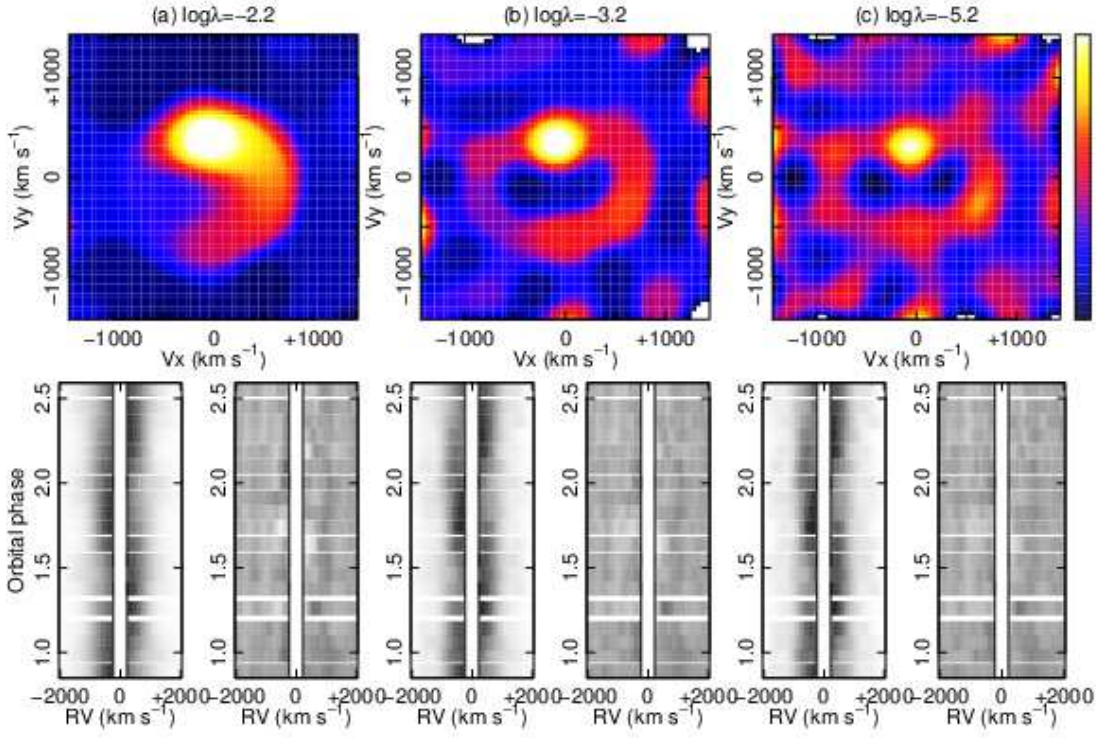

Fig. 9. As in figure 7, but for the data of WZ Sge whose absorption core is corrected by adding a Gaussian component.

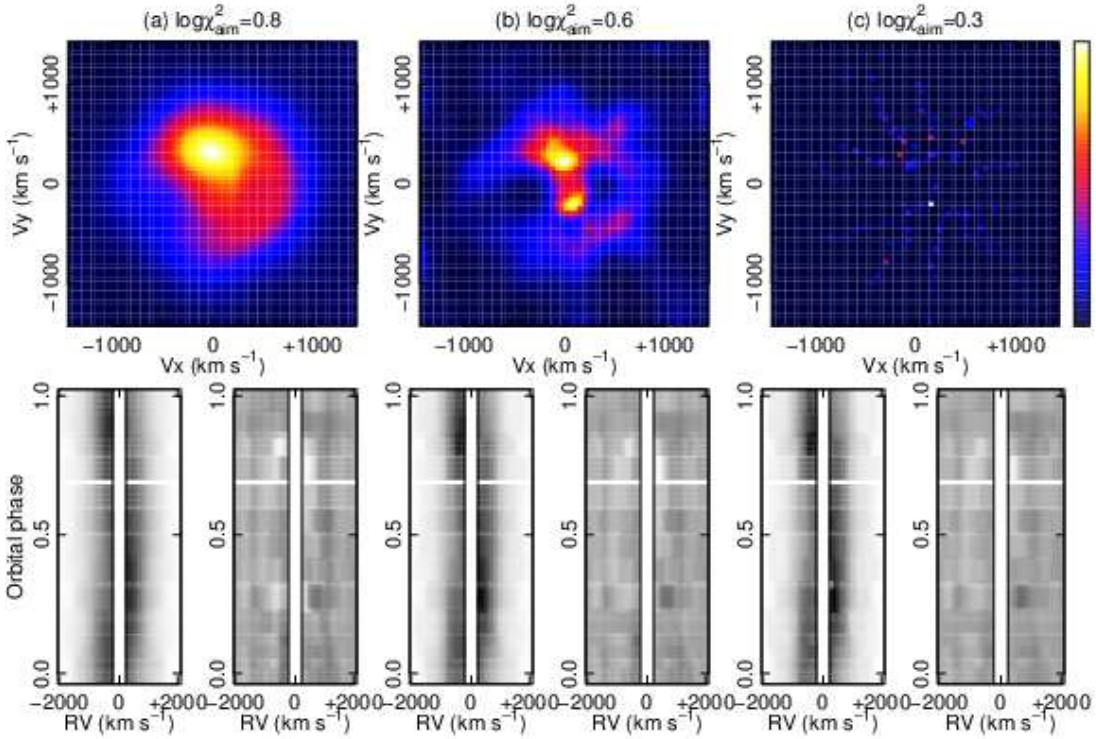

Fig. 10. As in figure 9, but for the MEM case.

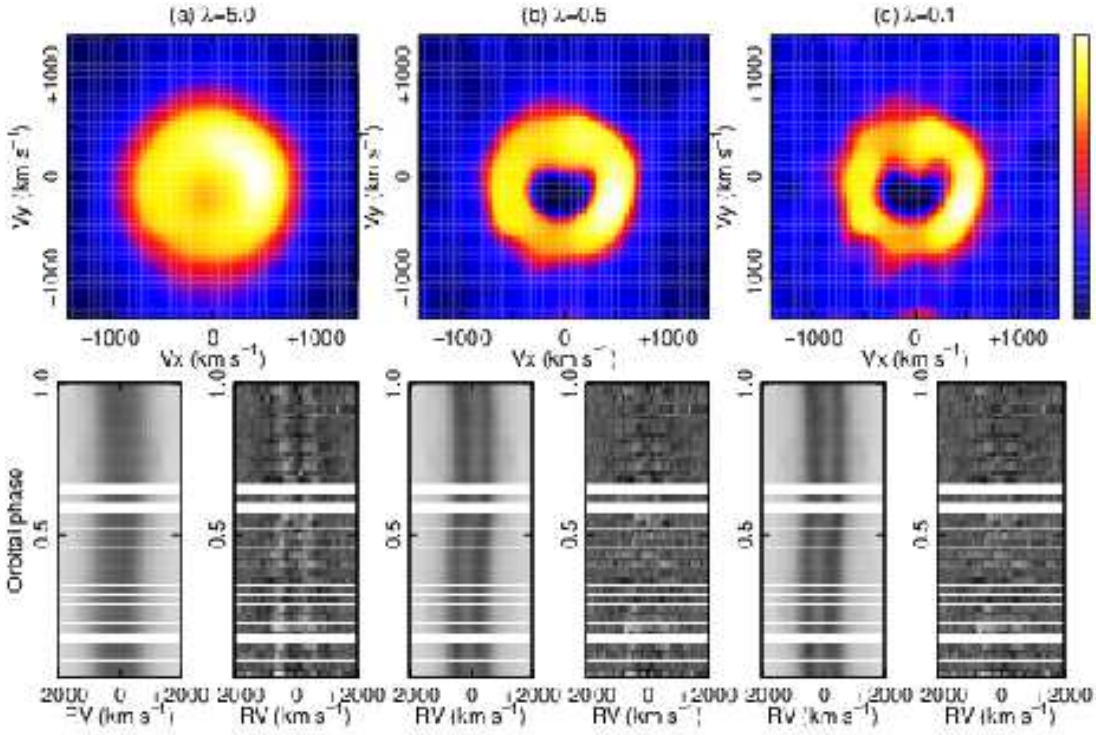

Fig. 11. As in figure 7, but for the data of TU Men.

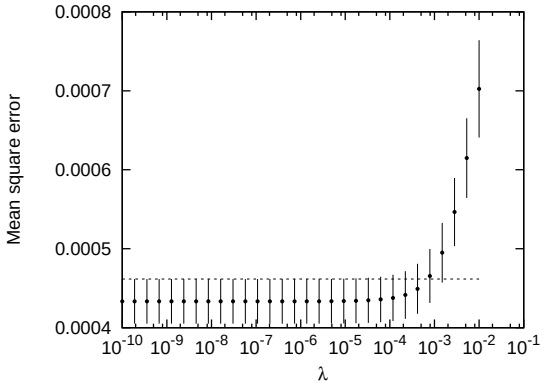

Fig. 13. The same as figure 12, but for the data of WZ Sge. The dashed line indicates the MSE at $\lambda = 10^{-7}$.

maps even in the case that the number of data is much smaller than the number of pixels of the map. Hence, this model is advantageous for the reconstruction of highly localized or edge structures in the Doppler map, such as the emission from the secondary star, hot spot, or shock wavefront.

Applications to the real data of WZ Sge and TU Men suggest that DTTVM can reconstruct the observed spectra with a high accuracy. As shown in subsection 3.2, we confirmed that DTTVM can provide the Doppler maps which are consistent with those by MEM. On the other hand, compared with the TVM maps, the MEM maps were more sensitive to the values of hyper-parameter: The maps tend to be very noisy with the hyper-parameter ($\chi^2_{\rm aim}$ in `doppler`) below a threshold. This is a common feature in `doppler` and `dopp`. The correction for the absorption core can also change the feature of the maps, as shown in the case of the data of WZ Sge (figures 8 and 10). The dependency on those factors was relatively low in DTTVM (figures 7 and 9). In conjunction with the cross-validation method, DTTVM can provide robust estimates of the Doppler map, compared with the MEM methods, especially in the case of that the number of data is small.

DTTVM can fit the absorption core by taking negative values of $\boldsymbol{s}$. However, it breaks the assumption of the Doppler tomography that all line sources rotate with the orbital motion of the binary. It is not evident whether the Doppler map can be deformed by the presence of absorption core. We performed a simple experiment using the artificial data. We assumed a Doppler map having a disk and spot, which is similar to figure 5, but the velocity of the disk center is set to be $(v_x, v_y) = (0, 0)$ in this case for simplicity. The observed trailed spectra were simulated from the map. Then, we added the absorption core to the spectra, and estimated the map by DTTVM. We assumed a periodic variation in the depth of the absorption component, in other words, the amplitude was proportional to $\sin(\phi)$. The amplitude variation was assumed in order to see how DTTVM behaves when the strength of the absorption core depended on the phase. Figure 14 shows the estimated map, model and residuals of spectra. The negative region appears at the center of the map. Compared with figure 5, the general features of the assumed disk and spot is unchanged by the presence of the absorption core. The spectral residuals clearly indicate the assume variation of the absorption component. The result of this experiment suggests that the model reconstructed the average absorption profile without significant change in the disk and spot features.

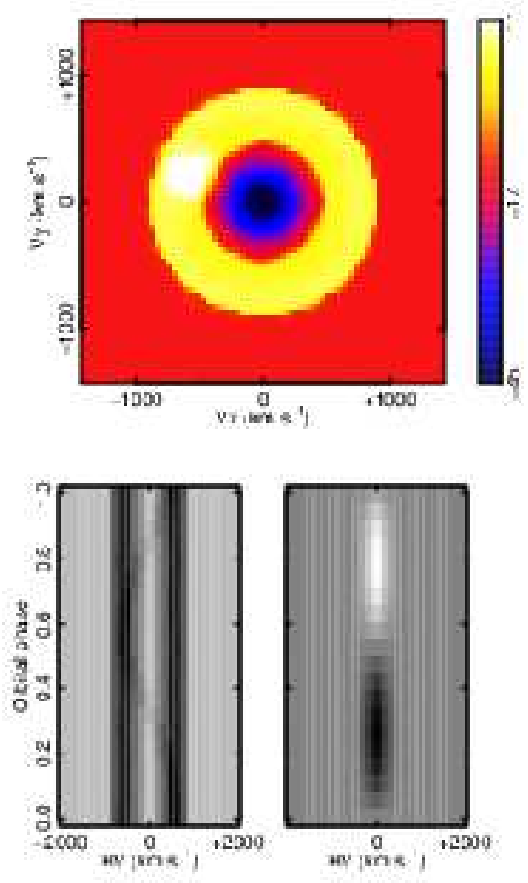

Fig. 14. The upper panel: Doppler map estimated from the spectra with an absorption core. The lower panels: the model (left) and residuals (right) of spectra. The assumed map is the same as figure 5.

5. Summary

We have developed a new model of the Doppler tomography using total variation minimization (TVM). This method can reconstruct localized features possibly having sharp-edges in the Doppler map, such as the emission from the secondary star, hot spot, and shocked region. This characteristics are emphasized in the case that the number of the data is much smaller than the number of pixels in the Doppler map. We applied it to the data of WZ Sge and TU Men. The model reproduces the observed spectra with a high precision. We demonstrated that reasonable values of the hyperparameter in our model can be estimated by the data itself using cross-validation.

This work was supported by JSPS KAKENHI Grant Number 22540252 and 25120007. We appreciate comments and suggestions from Dr. Shiro Ikeda and anonymous referee. REM acknowledges support by Fondecyt grant 1110347 and the BASAL Centro de Astrofisica y Tecnologias Afines (CATA) PFB–06/2007.

References

Bioucas-Dias, J. M. & Figueiredo, M. A. 2007a, Image Processing, IEEE Transactions on, 16, 2992

Bioucas-Dias, J. M. & Figueiredo, M. A. 2007b, in Image Processing, 2007. ICIP 2007. IEEE International Conference on Vol. 1 (IEEE), pp I–105

Chambolle, A. 2004, Journal of Mathematical Imaging and Vision, 20, 89

Harlaftis, E. T. & Marsh, T. R. 1996, A&A, 308, 97

Marsh, T. R. 2001, in Astrotomography, Indirect Imaging Methods in Observational Astronomy, ed. H. M. J. Boffin, D. Steeghs, & J. Cuypers (Springer-Verlag), 1

Marsh, T. R. & Horne, K. 1988, MNRAS, 235, 269

Marsh, T. R., Horne, K., Schlegel, E. M., Honeycutt, R. K., & Kaitchuck, R. H. 1990, ApJ, 364, 637

Mennickent, R. E. 1995, A&A, 294, 126

Nogami, D. & Iijima, T. 2004, PASJ, 56, 163

Schwope, A. D., Mantel, K., & Horne, K. 1997, A&A, 319, 894

Smak, J. 1981, Acta Astron., 31, 395

Spruit, H. C. 1998, arXiv:astro-ph/9806141

Steeghs, D. 2004, Astronomische Nachrichten, 325, 185

Steeghs, D., Harlaftis, E. T., & Horne, K. 1997, MNRAS, 290, 28P

Tappert, C., Mennickent, R. E., Arenas, J., Matsumoto, K., & Hanuschik, R. W. 2003, A&A, 408, 651

Young, P., Schneider, D. P., & Shectman, S. A. 1981, ApJ, 245, 1035